A Simple Picture for the Rotational Enhancement of the Rate for the F + HCl → HF + Cl Reaction: A Dynamical Study Using a New ab initio Potential Energy Surface†

Michael Y. Hayes,‡,§ Michael P. Deskevich,‡,|| David J. Nesbitt,‡,|| Kaito Takahashi,§ and Rex T. Skodje*,‡,§

Department of Chemistry and Biochemistry, University of Colorado, Boulder Colorado 80309, Institute of Atomic and Molecular Sciences, Academia Sinica, P.O. Box 23-166 Taipei, Taiwan, and JILA, University of Colorado and National Institute of Standards and Technology, Boulder, Colorado 80309

Received: June 30, 2005; In Final Form: September 6, 2005

Quantum scattering calculations for the reaction F + HCl → HF + Cl are performed on a new ground-state ab initio potential energy surface. The reagent rotation is found to have a dramatic effect on the reaction probability. Furthermore, the exit channel rotational thresholds leave a strong imprint on the reaction probabilities and even on the cumulative reaction probability. A very simple vibrationally adiabatic model is shown to account for most aspects of the reaction dynamics. In this model, the fast vibrational motion is adiabatically eliminated leaving the key reaction dynamics represented by a reduced atom + rotor collision. The shape of the adiabatic potential surface immediately yields to a simple and intuitive interpretation for the rotational enhancement of the rate. The rotational enhancement is shown to be an effect of the entrance channel dynamics of the atom−rotor problem.

Introduction

The reaction F + HCl → HF + Cl represents an important system for the study of chemical reaction dynamics because it is among the simplest examples of an asymmetric and highly exothermic "heavy−light−heavy" (HLH) reaction. The dynamics of HLH reactions have been studied extensively, as many important hydrogen atom (or proton) transfer reactions fall within this category (see review in ref 1 for work before 1993). On a fundamental level, HLH reactions have been of continuing interest to theorists since they generically exhibit a variety of fascinating dynamical behavior. For example, quantum tunneling is known to dominate the rate for many thermal HLH reactions. Also, HLH systems often support a rich spectrum of reactive resonances due to the existence of deep wells in the dynamical potential surfaces. There have been numerous studies of the related O(^{3}P) + HCl → OH + Cl reaction,[2−13] which has become a prototype system for asymmetrical HLH reactions. A comparison between this earlier work and the present results for the lower-barrier F + HCl reaction should provide useful insight into the generic behavior expected for this class of reactions. This is especially interesting since the F + HCl reaction is very exothermic while O(^{3}P) + HCl is nearly thermoneutral. The central focus of the present work is to probe the influence of reagent rotational excitation on the reaction dynamics and also to study the closely related issue of product rotational distributions. A strong enhancement of the reaction probability for rotationally excited reagents has been reported for O(^{3}P) + HCl.[7] As we will see, this behavior is even more pronounced for F + HCl. We present a simple and predictive model of the enhancement effect that we believe can help interpret the dynamics of many HLH systems.

The earliest detailed study of the F + HCl reaction was performed by Polanyi and co-workers,[14] who monitored the chemiluminescence of the HF product. They then constructed a London−Eyring−Polanyi−Sato (LEPS) potential energy surface (PES) with a small classical barrier of 1.1 kcal/mol in efforts to reproduce experimental data using classical trajectory simulations. Important kinetic data have been produced by Würzberg and Houston[15] for F + HCl and several related HLH reactions. The measured thermal rate constant of 8.1 (± 0.5) × 10^{-12} cm^3/s·molecule at $T = 300$ K is consistent with a moderate reactive cross section of about ∼1 Å^2. The temperature dependence of the rate constant exhibited significant non-Arrhenius behavior that was tentatively attributed to the formation of collision complexes. Kinetic data collected using other experimental techniques for this system have been generally consistent with the results of Würzberg and Houston.[16,17] The nascent ro-vibrational product distribution under thermal conditions has been measured by Polanyi and co-workers.[14] The reaction exothermicity of $\Delta D_0 = -33.2$ kcal/mol was found to be deposited largely into product vibration, with HF($v' = 2$) being the most highly populated state. Arrested relaxation measurements as a function of flow rate suggested that the products are rotationally hot, with a distribution peaking near $j' = 10$. Fully collision free experiments for F + HCl reactive scattering with supersonically cooled reagents have been recently performed in a crossed jet configuration, based on Doppler-resolved direct IR laser absorption of the nascent HF-(v', j') states.[18]

Theoretical work on the F + HCl reaction has also been ongoing. Last and Baer calculated a diatomics-in-molecules (DIM-3C) PES that predicted a barrier height of 4.0 kcal/mol.[19] More recently, ab initio calculations at 311G(3d2f,3p2d)-level were carried out using the PUMP2/PUMP4 method for 3400 geometries by Sayos et al.[20] The $^2A'$ state was then fit to a global analytical function. While the ab initio calculation originally predicted a barrier height of 4.0 kcal/mol at the highest level,

† Part of the special issue "Donald G. Truhlar Festschrift".

* Corresponding author e-mail: skodje@spot.colorado.edu.
‡ Department of Chemistry and Biochemistry, University of Colorado.
§ Institute of Atomic and Molecular Sciences, Academia Sinica.
|| JILA, University of Colorado and National Institute of Standards and Technology.

10.1021/jp0535745 CCC: $33.50
Published on Web 10/18/2005

TABLE 1: Properties of the DHSN−PES Transition State along with Those for the Sayos−PES[a]

	$V^{\neq}$ kcal/mol	V^{ad} kcal/mol	$V^{ad} - \epsilon_0^{bend}$ kcal/mol	∠FHCl	r_{FH}/a_0	r_{FHCl}/a_0	ω_{ss} cm^{-1}	ω_{bend} cm^{-1}	ω_{rxn} cm^{-1}
DHSN−PES	3.80	3.46	3.03	123.52°	2.69	2.51	2196.8	293.4	1113.3*i*
Sayos−PES	1.12	0.01	−0.26	131.2°	2.60	2.48	2094.4	189.0	1219.8*i*

[a] All energies are expressed with relative to the minimum of the entrance channel potential. $V^{\neq}$ is the classical barrier height relative to the reagents, V^{ad} is the adiabatic barrier height, and $V^{ad} - \epsilon_0^{bend}$ is the adiabatic barrier height neglecting the bend zero point energy. Adiabatic barrier heights were not available for the Sayos−PES, so we simply subtract the harmonic normal mode zero point energies to estimate the adiabatic barrier.

the barrier was empirically scaled downward to 1.1 kcal/mol to obtain agreement between the experimental rate constant and the predictions of transition state theory. The Sayos−PES has been used for classical trajectory simulations of the reaction under thermally averaged reagent collision conditions.[21] The same surface has also been used by Tang et al.[22] for a time-dependent wave packet study of the reaction dynamics. As an extreme limiting case, the most recent study of this reaction has been a quasi-classical trajectory (QCT) study by Kornweitz and Persky on a new LEPS−PES with a zero barrier height to reaction.[23]

The PES of Sayos et al.[20,21] and the LEPS surfaces are empirical, in the former case at least to the extent that the barrier height was adjusted to experiment. A high level ab initio surface (DHSN−PES) has been recently produced by Deskevich et al.[24] This was based on dynamically weighted, complete active space MRCI + Q calculations using a series of AV*n*Z ($n = 2, 3, 4$) basis sets, with the complete basis set limit (CBS) achieved by extrapolation methods of Peterson and co-workers.[25,26] The lowest three electronic state energies (2A′, 1A″) have been calculated at 3230 geometries, with the resulting ground-state energies fit to the analytic expansion of Aguado and Paniagua.[27] Even at this much higher ab initio level, the barrier height on the DHSN−PES remains higher (3.80 kcal/mol) than previous empirical surfaces, and the saddlepoint geometry is highly bent. In this first paper, we explore dynamics of F + HCl on this DHSN−PES, with the aim of developing a physical understanding of rotational effects in HLH reactions. A more detailed description of the DHSN−PES surface construction as well as explicit comparison between theoretical and experimental results will be presented later in a companion work.[28]

As shown below, the influence of reagent rotational excitation on the reaction probabilities for F + HCl is quite profound. At a total energy equal to about 2 kcal/mol above the threshold energy, the $J = 0$ reaction probability is highest for the HCl($v = 0, j = 9$) state, which is over 100 times larger than that for HCl($v = 0, j = 0$). While the influence of rotational excitation on reaction rates has been discussed many times for individual reactions, the range of observed behavior is very diverse.[29] In many systems, reagent rotational excitation can inhibit reactivity since it deflects the colliding complex from the optimal reaction path. When rotation does promote reaction, the effect can be highly dependent on translational energy and the orientational state of the rotor. Many aspects of this behavior have been discussed in the context of the "stereodynamics" of chemical reactions.[30]

The rotational enhancement/suppression of a reaction should be viewed as a consequence of entrance channel dynamics. Thus, rotation will influence the probability that the colliding pair will reach the transition state (TS) dividing surface but does not generally have a strong effect on the subsequent recrossing probability. Loesch[31] emphasized the role of the entrance channel rotational-translational (RT) dynamics by plotting classical trajectories in the Jacobi (R, γ) space up to the dividing surface. Some time ago, we introduced a vibrationally adiabatic model that explicitly converts a HLH reaction into a rotational scattering problem.[1,32−35] This model is based on the clear separation of time scales between the slow RT motion and the fast vibration and permits the elimination of the fast motion. In classical mechanics, the reaction probability (P_R) for a given initial state is then proportional to the probability of crossing a carefully defined critical dividing surface to reaction. In quantum mechanics, the P_R for symmetrical HLH systems can be obtained from a coherent superposition of *g*-parity and *u*-parity solutions to the RT scattering problem that also includes the exit channel RT dynamics.[34,35] Smith and co-workers have developed the kinematic-mass model (KMM)[36,37] that yields useful insight into the reduced RT scattering problem. On the basis of the earlier line-of-centers treatment, the KMM assumes straight-line trajectories up to the dividing surface. The rotation enhancement observed in QCT simulations of the O(^{3}P) + HCl reaction could then be explained in terms of the alignment of the velocity vector of the RT motion of the reagents with the normal vector to the dividing surface.

The remainder of this paper is organized in the following way. In the Theoretical Simulation section, we describe the computational methods used for the dynamical calculations and also review the potential energy surface. The detailed results of the classical and quantum simulations are also presented in this section. In the Analysis section, we present the adiabatic model used in the analysis of the raw simulation data. The physical interpretation of the rotational enhancement effect is shown to be particularly simple when viewed in terms of the adiabatic model. Further details of the reaction dynamics are likewise interpreted in terms of the model. In the last section, we summarize our findings and discuss their implications.

Theoretical Simulation of the F + HCl Reaction

DHSN−PES. As mentioned in the Introduction, the present study of the F + HCl reaction employs the DHSN−PES. Therefore, we begin with a short review of the essential features of this surface. The PES is based on extensive quantum chemistry calculations using the MOLPRO suite of ab initio programs.[38] The three-state (2A′, 1A″) full valence MRCI + Q wave functions were calculated using reference configurations from a six-state (4A′, 2A″) dynamically weighted MCSCF calculation.[39] The adiabatic energies were extrapolated to the complete basis set (CBS) limit using the standard AV*n*Z atomic basis sets ($n = 2, 3, 4$). Finally, correlation energies were scaled (by < 3%) to accurately reproduce the experimental reaction exothermicity, with the same correlation scaling factor applied consistently to all points on the surface. The calculations were performed at 3230 geometries and numerically fit to the analytic form of Aguado and Paniagua,[27] with an rms deviation of < 0.1 kcal/mol along the reaction path.

In Table 1, we present some of the characteristics of the final fitted surface. The barrier height is 3.80 kcal/mol relative to

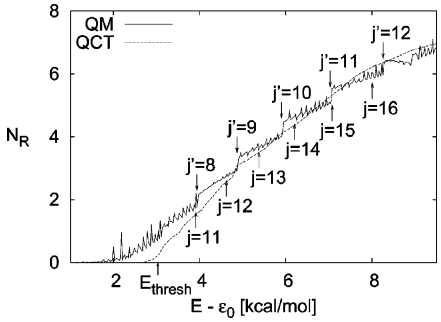

Figure 1. Quantum mechanical (solid line) and quasiclassical (dashed line) cumulative reaction probabilities for F + HCl for $J = 0$ (N_R^0); the total energy is defined relative to the reagent zero point energy (ϵ_0). Reagent and product state threshold energies are indicated with arrows.

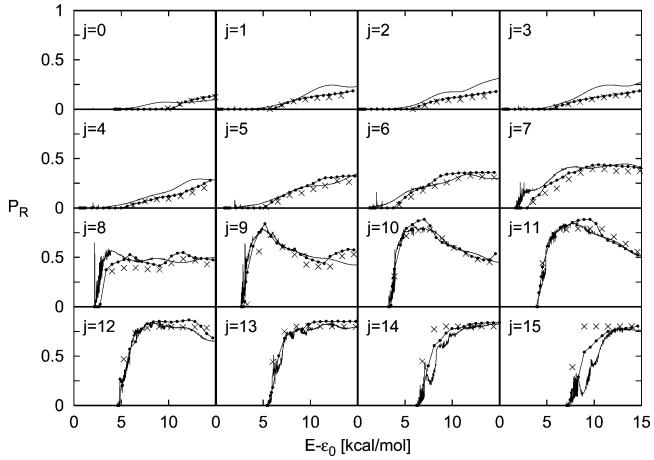

Figure 2. Quantum mechanical (solid lines), quasi-classical (lines with points), and vibrationally adiabatic (symbols) final state summed reaction probabilities for F + HCl($v = 0$, j); total energy is relative to the reagent zero point energy.

the entrance channel well. The transition state geometry is highly bent, with ∠FHCl = 123.5°. As would be expected, the position of the transition state is "early" so the HCl bond length is close to its equilibrium value. The harmonic vibrational frequencies at the saddlepoint are 2196.8 and 293.4 cm^{-1}. The ground state vibrationally adiabatic barrier, computed using harmonic zero point energies, is shifted slightly toward reagents and found to be at 3.46 kcal/mol based on a reaction path calculation. If the bending zero point energy is neglected (see below), the adiabatic barrier is 3.03 kcal/mol. For reference, we have also included the corresponding information for the empirically adjusted PES of Sayos et al.,[20,21] which has a 2.68 kcal/mol lower classical barrier height

Quantum Scattering Calculations. Quantum scattering calculations were performed using the time-independent, close-coupled hyperspherical method of Manolopoulos and co-workers.[40] The first set of calculations were carried out for total angular momentum $J = 0$. The *S*-matrix elements were generated on a fine grid of energies spaced by 1 meV extending up to a total energy of 0.955 eV above the classical minimum energy of the reagents. The cutoff energy for truncation of the surface states was chosen to be 2.55 eV. The rotational basis set included states up to $j = 25$. The hyperradial wave function was propagated from $\rho = 4.85$ to $\rho = 45.0$ a_0 in 560 steps. The results are converged with an error of less than 1%. The next set of calculations were for $J = 1-4$ over the same range of energies. A full helicity basis was used, but otherwise the convergence parameters in the computation were chosen to be the same. Since these calculations were time-consuming, fewer total energies were calculated. Higher values of J were not calculated.

The cumulative reaction probability for $J = 0$ (N_R^0) is plotted in Figure 1 versus shifted total energy. [For the remainder of this paper, energy refers to total energy relative to the HCl zero point energy on this surface (4.27 kcal/mol), unless indicated otherwise.] We define

$$N_R^J(E) = \sum_{\substack{v,j,k \\ v',j',k'}}^{\text{open}} P_R(v, j, k \rightarrow v', j', k'; E; J) \qquad (1)$$

where P_R is the square magnitude of the *S*-matrix elements and (v, j, k) (or (v', j', k')) represent the reagent (or product) vibrational, rotational, and helicity quantum numbers labeling the channel. There are a number of interesting features exhibited by $N_R^0(E)$. First, the effective threshold in $N_R^0(E)$, empirically defined as $N_R^0(E_{thresh}) = 0.5$, lies at 2.95 kcal/mol. This represents a significant dynamical reduction from the full adiabatic barrier height, which occurs at 3.46 kcal/mol. On the other hand, if the bending zero point energy is neglected, the adiabatic barrier lies at 3.03 kcal/mol and is roughly consistent with E_{thresh}. Next, we note the existence of a dense resonance spectrum that is distributed over the entire energy range considered. At low energies, as seen in Figure 1, most of the reaction appears to be mediated through the resonance states. Intricate resonance structure has been similarly observed for O(^{3}P) + HCl[7−10] and many other HLH systems.[33,41−44] Xie et al.[11] have recently been able to assign a number of states in O(^{3}P) + HCl to van der Waals type states in the entrance and exit channels of the reaction. But in contrast, the F + HCl reaction shows a resonance spectrum that more clearly extends to high energy. Finally, the most interesting feature of $N_R^0(E)$ is the occurrence of a sharp step structure versus energy. Normally, the staircase structure of $N_R^0(E)$ observed in other reactions is much less distinct (due to tunneling) and reflects the sequential opening of quantum bottleneck states at the transition state. In those cases, the energy positions of the steps are determined from the energies of vibrationally excited states of the activated complex.[45] The structure observed in Figure 1 is completely inconsistent with this interpretation. The steps are much sharper that they should be based on estimated tunneling through the adiabatic barriers. Furthermore, the positions of the observed steps do not correlate in any clear way with the transition state vibrational frequencies. Instead, the energy positions of the steps appear to correspond to the diatomic rotational energy levels. In Figure 1, the threshold energies for F + HCl($v = 0$, j) and Cl + HF($v' = 3$, j') are indicated. The step positions almost precisely match the exit channel threshold energies.

A more detailed picture of the reaction dynamics is provided by the state-selected reaction probabilities. The total (final state summed) reaction probability at a given J is defined as

$$P_R(v, j) = \frac{1}{2j+1} \sum_{\substack{k \\ v',j',k'}}^{\text{open}} P_R(v, j, k \rightarrow v', j', k') \qquad (2)$$

and measures the total reactivity from a given ro-vibrational reagent state. [For $J = 0$, the helicity averaging and the $(2j+1)$ prefactor drop out of this expression.] In Figure 2, we show the $J = 0$ results $P_R(j) \equiv P_{R(}v = 0, j)$ for a number of initial rotational states. The rotational enhancement of the reaction is clear from this plot. The reaction from the ground state ($P_R(0)$)

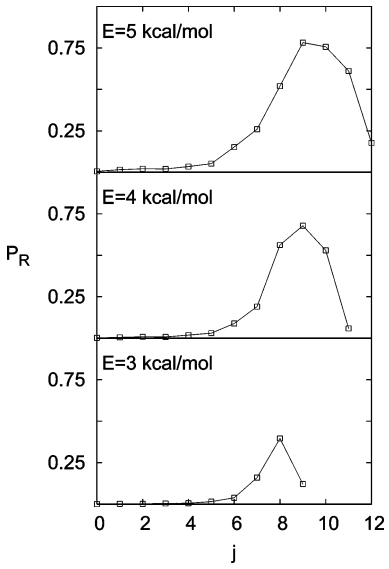

Figure 3. Rotational enhancement effect for F + HCl($v = 0$, j). The final state summed $J = 0$ reaction probabilities vs reagent rotational level (j) are shown for fixed total energy. The results for several total energies (relative to the reagent zero point energy) are depicted.

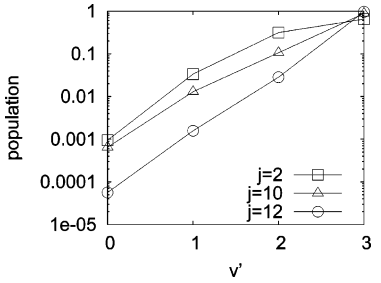

Figure 4. Product vibrational distribution for ($J = 0$) F + HCl($v = 0$, j) with $j = 2$, 10, and 12 for $E - \epsilon_0 = 5$ kcal/mol.

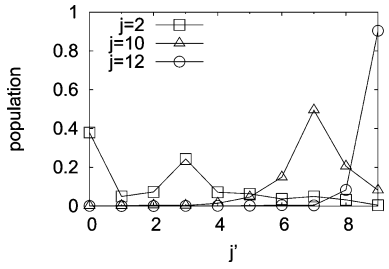

Figure 5. Product rotational distribution for ($J = 0$) F + HCl($v = 0$, j) with $j = 2$, 10, and 12 for $E - \epsilon_0 = 5$ kcal/mol and $v' = 3$.

is negligible at the nominal threshold energy of 2.95 kcal/mol and never rises above 0.1 for any energy considered. Indeed, the reactivity of all the reagent states with $j < 5$ is found to be quite low. In contrast, the high-j states ($j \geq 8$) are very reactive, with P_R often rising above 0.5. The effective thresholds for reactivity move lower in total energy as j increases from 0 up to 7. In Figure 3, the total reactivity at several values of total energy is plotted versus the reagent quantum number j. The preference for the high-j states is clear at all energies.

The product state distributions versus energy for several initial reagent states are presented in Figures 4 and 5. The total vibrational distribution (j'-summed) shows a preference for $v' = 3$, with the $v' = 0$ state negligibly populated. The rotational distributions for high initial j, restricted to the dominant $v' = 3$ product manifold, are uniformly hot. An intriguing observation can be made concerning the reactivity from the high-j initial

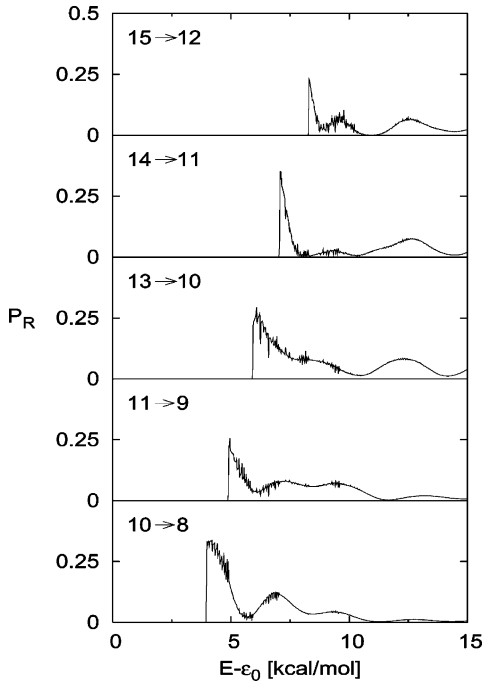

Figure 6. Dominant state-to-state transitions controlling the "step" formation in the cumulative reaction probability selected from the states F + HCl($v = 0$, $j \rightarrow v' = 3$, j').

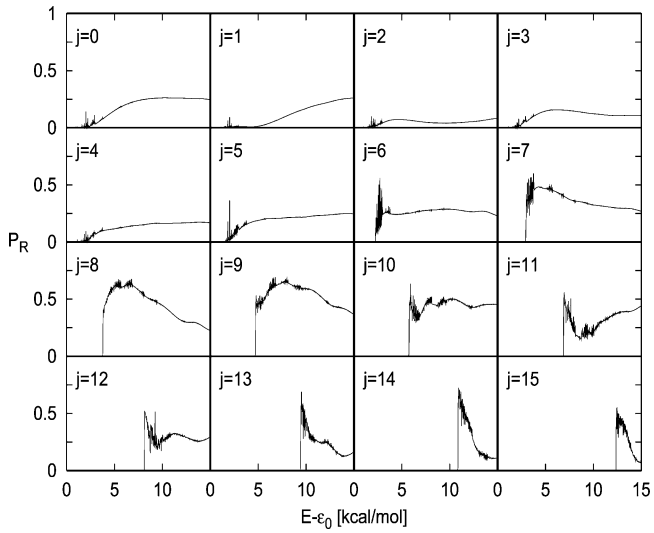

Figure 7. Quantum mechanical product-state summed reaction probabilities for the reverse reaction Cl + HF($v = 3$, j) → F + HCl(all) with $J = 0$; the collision energy is measured relative to the channel Cl + HF($v = 3$, $j = 0$).

states (that dominate the overall rate). Namely, at high-j the state-to-state reaction probabilities exhibit sharp thresholds for certain ($v = 0$, $j \rightarrow v' = 3$, j') transitions. These transitions follow a rough energy matching condition of the thresholds (i.e., E[F + HCl($v = 0$, j)] ≈ E[Cl + HF($v = 3$, j')]). The reaction probabilities for some of the dominant state-to-state transitions are shown in Figure 6.

We have also assembled the various reaction probabilities for the reverse reaction, Cl + HF → HCl + F, using microreversibility. As shown in Figure 7, total reaction probabilities for Cl + HF($v = 3$, j) → HCl + F exhibit extremely sharp dynamical thresholds at the threshold energies of the Cl + HF reagent states. The rotational enhancement effect for the HF($v = 3$) manifold is apparent from Figure 8 but is somewhat less pronounced than for the forward reaction.

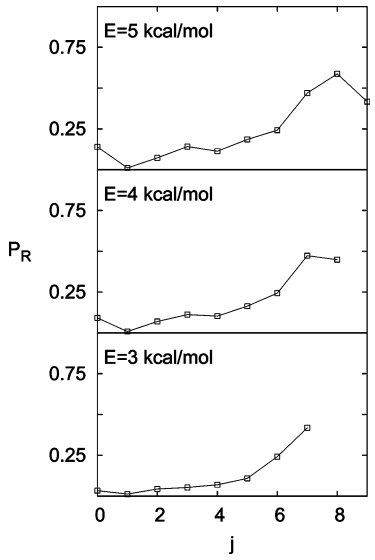

Figure 8. Total quantum reaction probability for Cl + HF($v = 3$, j) → F + HCl(all) vs j with $J = 0$ at several total energies measured relative to the Cl + HF($v = 3$, $j = 0$) channel.

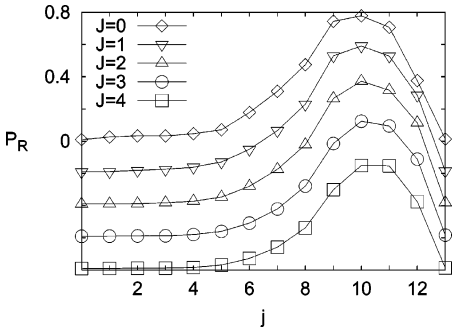

Figure 9. Final state summed quantum reaction probabilities for F + HCl vs j for different values of the total angular momentum, $J = 0-4$; the total energy is held fixed at $E - \epsilon_0 = 4.7$ kcal/mol. For clarity, each successive curve is displaced vertically by 0.2.

Finally, we discuss some results obtained for the F + HCl → HF + Cl reaction occurring at higher total angular momentum (J). In Figure 9, we plot the reaction probability as a function of j for the different values of total J. The rotational enhancement is almost identical for the higher values of J. Furthermore, the cumulative reaction probabilities obtained for $J > 0$ were found to be generally consistent with the predictions of a simple JK-shifting scheme adapted to this reaction. The main purpose of the $J > 0$ calculations was to determine if the $J = 0$ constraint of the original simulation produced unphysical artifacts in the described reaction dynamics. Our results show that, in fact, there is nothing particularly special about the $J = 0$ case and that the $J = 0$ simulations provide a reasonable basis to discuss low impact parameter scattering.

Classical Trajectory Simulations. To help identify purely quantum mechanical (QM) effects in the dynamics, we have also carried out quasi-classical trajectory (QCT) simulations of the reaction dynamics. For the most part, the calculations were implemented using standard methods. The initial conditions for the HCl($v = 0$, j) diatom were selected from a random sampling of the vibrational/rotational phases from trajectories exactly satisfying the semiclassical quantization conditions. The orbital and diatomic angular momentum vectors were chosen to exactly enforce the condition $J = 0$ following the method of Nakamura and co-workers.[9] The final quantum state populations were not extracted from the simulations.

We have plotted the results for the reactivity $P_R(j)$ obtained from the QCT simulations in Figure 2 for comparison to the quantum results. In these results, no final state binning is needed. It is seen that the QCT and quantum results are generally quite similar. The strong preference for high j-states is reproduced, as are the approximate positions of the thresholds to reactivity. Differences in the fine details are expected, as the resonance and tunneling effects are not accounted for by a QCT model. However, the QCT does account for the rotational enhancement effect, which is apparently a classical effect.

The QCT cumulative reaction probability was obtained by summing the QCT $P_R(j)$ over all open initial channels. As seen in Figure 1, the overall shape and scale of $N_R^0(E)$ is well-modeled by the classical mechanics. Again, the quantum tunneling and resonance effects are not reproduced. Despite the generally good agreement of QCT and QM for the P_R, the pronounced steps in $N_R^0(E)$ are only vaguely seen in the classical simulations. In view of the sharp state-to-state threshold behavior occurring at the product threshold energies in the QM simulation, we conjecture that the failure of the steps to appear clearly in the QCT simulations is the result of our neglect to include final state quantization conditions. It would be interesting to see if the use of a narrow Gaussian binning of the final ro-vibrational states could reproduce the staircase structure.

Analysis

Adiabatic Capture Model. Guiding insight into the dynamics of HLH systems is provided by a simple time scale analysis.[1,32−51] For a reaction HL + H′ → H + LH′, the diatomic vibrational motion is generally much faster than the RT motion in the entrance and exit channels. Likewise, near the TS the asymmetric stretch (as) frequency (ν_{as}) is much higher than that of the symmetric stretch (ν_{ss}). Typical values are $\nu_{as} \sim 10\nu_{ss}$. The bending motion (b) of the complex shows an intermediate time scale, typically $\nu_{as} \sim 3\nu_b$, that we have usually combined with the symmetric stretch as a slow variable so that it is treated without assuming that its action is conserved. [Since F + HCl has an early TS, the "asymmetric stretch" is very nearly the HCl vibration while the "symmetric stretch" closely resembles the translational coordinate.] In the present F + HCl reaction, the bending frequency is even lower, which even more strongly validates this grouping of time scales. Thus, we expect that the fast vibration can be globally eliminated using the adiabatic approximation leaving the translational-(as) + rotation-(b) dynamics as the template for the reaction. The difficulty with this picture is the reaction itself. Precisely at the barrier energy (when the light atom transfers between the heavy atoms) the fast asymmetric stretch frequency goes to zero heralding a classical separatrix crossing (or a quantum mechanical avoided crossing) and the breakdown of adiabatic theory. This separatrix crossing can lead to large and very rapid changes in the vibrational action (or quantum number). Previously, we have extensively discussed this problem and its solution, and so here we merely restate the results.[32,52−55] Using a composite set of entrance/exit channel Jacobi coordinates matched at a surface near the TS, the dynamics are mapped to a set of double well problems parametrized by (R, γ). The matching surface is most easily set to the ridge of the full PES that passes through the true saddlepoint. The eigenstates of the double well are found for all values of (R, γ), and the adiabatic potentials $\epsilon_n(R, \gamma)$ are the vibrational eigenenergies. If the full state-to-state dynamics is desired, then separatrix crossing theory must be invoked to follow the motion from the reagent state to the product state. This asymptotic matching process, however, is not required in the present problem.

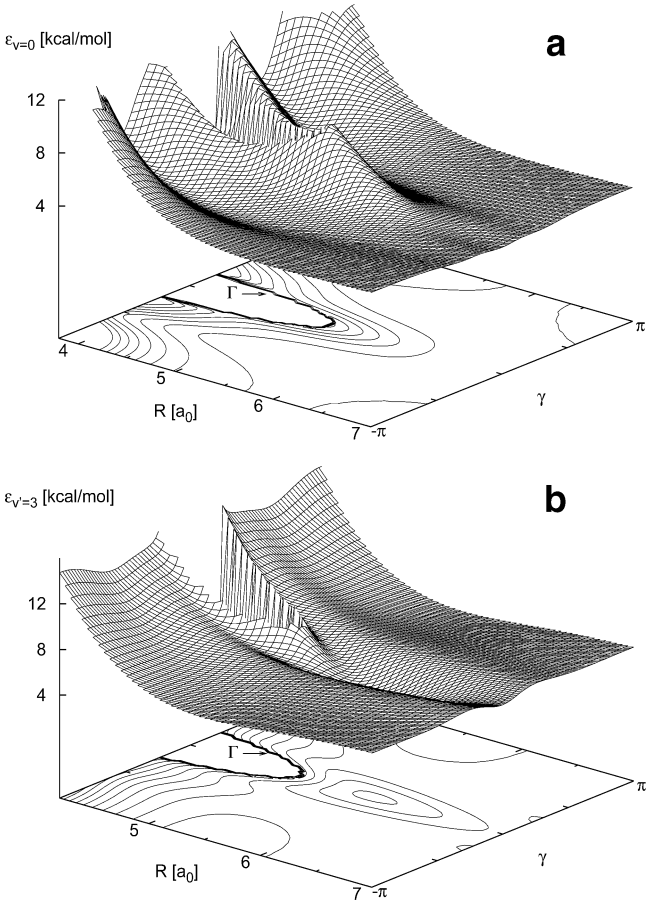

Figure 10. Vibrationally adiabatic potential surfaces. (a) The entrance channel surface for F + HCl($v = 0$), and (b) the exit channel surface for Cl + HF($v = 3$). The coordinates are the entrance/exit channel Jacobi coordinates for (a)/(b). The dividing surface (Γ) is indicated by the bold curve around $\gamma = 0$; the contour spacing is 1 kcal/mol. Here, and in Figure 11, the range of the γ coordinate is periodically extended from its natural range of $(0, \pi)$ to aid visualization.

In the entrance or exit channel, the dynamics is well represented by the RT Hamitonian

$$\boldsymbol{H} = \frac{P_R^2}{2M} + \frac{L^2}{2MR^2} + \frac{j^2}{2I(R,\gamma)} + \epsilon(R,\gamma) \qquad (3)$$

where the Jacobi coordinates (R, γ) are selected appropriately for the channel, M is the translational reduced mass, and $\epsilon(R, \gamma)$ is the adiabatic energy surface for the state of interest The coordinate dependence of the diatomic moment of inertia, $I(R, \gamma)$, is generally weak and can usually be neglected. Thus, the dynamics is that of a conventional rotational scattering problem with the potential $\epsilon(R, \gamma)$. In Figure 10, we show profiles of the $\epsilon(R, \gamma)$ computed for F + HCl($v = 0$) and Cl + HF($v' = 3$). The reaction is represented by passage into the deep wells situated at $\gamma = 0$ and small R. The incoming reagent flux must surmount the barriers guarding the wells for reaction to occur. The bent transition state is clearly seen as a saddlepoint on the F + HCl($v = 0$) surface. Ignoring recrossing effects, reaction is defined in this reduced dynamics as passage across a curve Γ that is situated along the barrier ridge in the (R, γ) plane.

To model the reaction, we assume that the dynamics is represented accurately by the RT Hamiltonian up to the critical surface Γ. Then, the "capture probability" ($P_\times$) can be defined as the reagent flux across Γ divided by the incident flux. It is numerically computed as the fraction of orbits from the ensemble that cross Γ when propagated using the Hamiltonian given by eq 3. The subsequent transmission probability of ultimate passage to products is represented by κ. Then we have the simple capture theory for the reaction probability:[56]

$$P_R(j) = \kappa P_\times \qquad (4)$$

In a previous study of the symmetrical I + HI reaction,[32] we have found that κ is reasonably approximated by the constant $\kappa = 0.5$ independent of energy and j. This behavior holds true in the present case as well, although detailed studies using eq 4 demonstrate ex posteriori that the value is approximately $\kappa = 0.8$. A larger value of κ is reasonable since F + HCl is a very exothermic reaction. The predictions of eq 4 are plotted in Figure 2, with $\kappa = 0.8$. It is seen that the capture model very well reproduces the full QCT results for all energies and all initial j-states. This result, along with a number of other comparisons of full QCT to the adiabatic capture theory leads us to believe that this simple picture of the reaction is accurate.

Adiabatic Dynamics of the F + HCl Reaction. We now consider the specific interpretation of the F + HCl reaction in terms of the adiabatic model. Since we have seen that the rotational enhancement effect is essentially classical in origin, we can proceed with a classical picture of the RT dynamics. (Of course the fast vibration is quantal through the representation of $\epsilon(R, \gamma)$). As κ is reasonably well-approximated by a constant for all reagent states, the origin of the rotational enhancement effect must be sought in the capture probability ($P_\times$). Thus, the essential issue is how the rotation of the reagent molecule affects the Γ-curve crossing dynamics taking place on the $\epsilon(R, \gamma)$ effective potential. In Figure 11, we show ensembles of trajectories with various initial rotational phases in the (R, γ) plane, corresponding to $j = 0$ and $j = 10$, but at the same total energy of 5 kcal/mol. Low-j trajectories approach the interaction region "vertically" while high-j trajectories approach the target along diagonal (or sideways) paths. The protruding ridge of the adiabatic potential is seen to steer away trajectories that impinge on the target with low-j, so very few trajectories cross the critical dividing surface Γ. High-j trajectories, on the other hand, make a more sideways attack on the barrier and are less deflected in their approach to Γ. Since the RT dynamics is easy to visualize, it is relatively straightforward to explain the behavior of the classical capture probability.

The preference for sideways barrier attack (i.e., the efficacy of rotational energy) can be explained in terms of two contributing mechanisms that can be observed in Figure 11. The first is a simple geometrical effect analogous to the familar cone of acceptance picture. A quasi-classical ensemble is composed of a distribution of trajectories with the initial rotational phases, $\gamma_0 \in (0, \pi)$. Ignoring the potential, a fraction these orbits (F) would cross the critical Γ-curve as they followed straightline paths in (R, γ). This fraction increases with j simply because the geometrical profile of the Γ-curve appears larger from the sideways direction. By itself, this purely geometrical effect significantly underestimates the rotational enhancement that is observed. The second contributing effect is the dynamical deflection of orbits away from the Γ-curve by the protruding potential ridge. Trajectories approaching the ridge from a vertical direction (low-j orbits) suffer much greater deflection and are far less likely to cross Γ than those that attack from the sideways direction (high-j orbits). The reason for this distinction is the shape of the potential along the differents paths of approach. Vertical trajectories are likely to impact the ridge in the vicinity of $\gamma = 0$ where the potential is highly convex, $d^2\epsilon/d\gamma^2 < 0$, and are thus strongly deflected away from the "target" Γ.

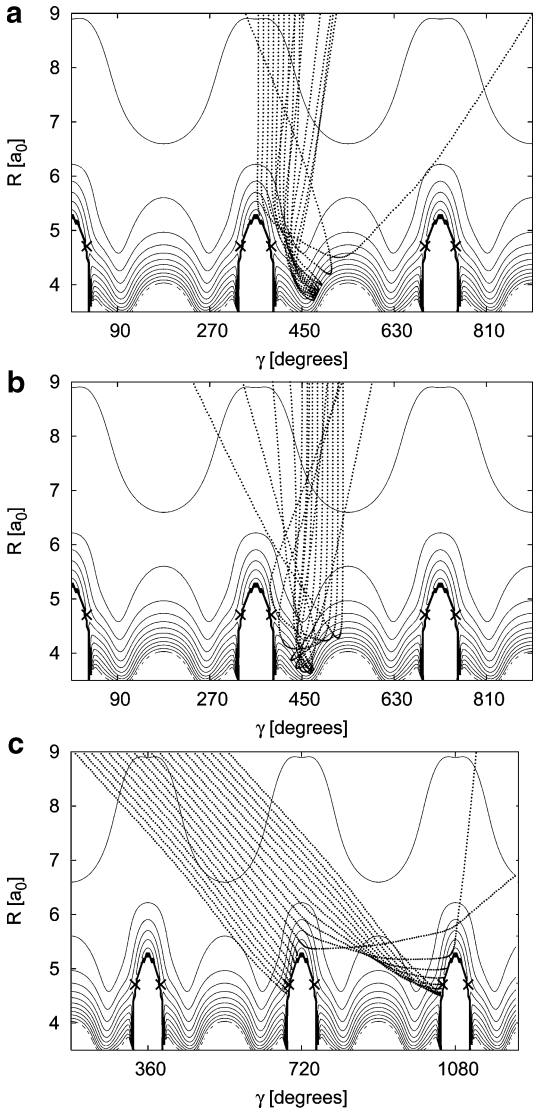

Figure 11. Ensembles of classical trajectories on the adiabatic entrance channel potential ($E - \epsilon_0 = 5$ kcal/mol, $v = 0$, $J = 0$). The saddle points on the adiabatic potential are marked with ×. Vertical ($j = 0$) trajectories are deflected from the large ridge (a) but are steered toward a reactive geometry by the smaller ridge (b). Diagonal ($j = 10$) trajectories (c) mostly follow straight paths to reaction, as they move parallel to the steering force of the ridge.

Dynamically, the motion is highly unstable and is characterized by a large local Lyapunov exponent. Thus, while the vertical trajectories have sufficient energy to surmount the barrier, the instability inhibits the system from reaching the critical configuration and therefore attenuates the reaction probability. By contrast, along the sideways approach, the potential is flat or slightly concave with respect to displacements perpendicular to the orbit and is thus far less unstable. Therefore, a higher fraction of high-j trajectories will proceed undeflected across Γ.

Most of the observed rotational enhancement effect is understood in terms of the direct barrier climbing dynamics just described. In the simplest terms, for high-j states, most of the energy required to climb the adiabatic barrier is provided by rotation. Stated differently, the reaction coordinate has a large rotational component. Not coincidently, the magnitude of $P_R(j)$ near threshold (see Figure 2) grows rapidly once the rotational energy approaches the adiabatic barrier height (around $j = 8$). However, a full quantitative description of the reactivity must also include indirect processes. For example, the trajectory may scatter sideways from the potential ridge and undergo a complete internal rotation before crossing Γ. Other trajectories may first strike the small backward protrusion of the potential at $\gamma = 180°$ and scatter across Γ. While such indirect (multiple scattering) processes are relatively weak, they do play a significant role in the reactivity of low-j states at higher translational energies.

Finally we note that the RT dynamics generated by the adiabatic model is also adequate to explain the ultimate decrease in reactivity of very high-j states. When E_{tot} is held fixed, the very high-j states are characterized by $E_{rot} \gg E_{trans}$, and thus incident trajectories move nearly horizontally in the (R, γ) plane. Such trajectories repeatedly encounter the repulsive tip of the potential barrier and deflected back to large R before the Γ-curve is encountered.

Adiabatic Dynamics of the Cl + HF Reaction. While the rotational enhancement is an entrance channel phenomenon, we have noted that threshold energies of the Cl + HF($v' = 3$, j') channels nearly perfectly define the step positions in the cumulative reaction probability $N_R^0(E)$. Since $N_R^0(E)$ is rigorously equal for the forward and backward reactions, these steps must then also relate to entrance channel threshold effects for the reverse reaction. Therefore, we shall consider the behavior of the endothermic Cl + HF → F + HCl reaction using the adiabatic model. To limit the discussion, we only consider a few aspects of the Cl + HF($v = 3$) case.

The same methodology is invoked to study the Cl + HF reaction via the adiabatic capture model as was used for the forward reaction. However, as seen in Figure 10, the adiabatic potential surface for the reverse reaction is vastly different than that for the F + HCl($v = 0$) reaction. The critical Γ-curve has roughly the same shape as the forward reaction. However, the protruding ridge seen in Figure 10a is replaced by a deep adiabatic well in Figure 10b. The well is slightly shielded by a very small barrier ridge that can easily be overcome either through translational or rotational energy.

As expected, the RT dynamics exhibited by Cl + HF($v = 3$, j) collisions is quite different from that occurring for the forward reaction. In order for trajectories to cross the Γ-curve, they first encounter the surrounding adiabatic well. If the trajectories possess sufficient initial kinetic energy, they are relatively unaffected by the well (depth ∼2 kcal/mol) and accelerate directly to the Γ-curve. Due to the absence of the large protruding potential ridge, there is little attenuation by trajectory instability. For moderate or high kinetic energies, the trajectories are thus not appreciably deflected, and the rotational enhancement is due solely to the geometrical effect. This explains the more modest rotational enhancement effect observed in the QM simulations of Cl + HF($v = 3$, j) as compared with the forward reaction. Near threshold, however, the adiabatic well does significantly affect the trajectory dynamics. Low-j trajectories ($j = 0$, 1) with near-threshold translational energies can be trapped in the adiabatic well. At higher j, the near-threshold trajectories tend not to trap in the well per se but are translationally accelerated toward collision (i.e., toward smaller R) by the influence of the attractive well. For sufficiently low collision energies, the HCl diatom will undergo several complete rotations under the strong attractive force from the adiabatic well. Such trajectories can eventually acquire as much as 2 kcal/mol of translational energy. After being translationally accelerated, the trajectories undergo a strong collision, and those orbits that are properly aimed will cross the Γ-curve and react. Since the saddlepoint of $\epsilon(R, \gamma)$ lies about 0.5 kcal/mol above the asymptote, a fraction of the barrier climbing energy must also

be provided by rotation. Thus, due to the attractive well, the reaction probability is large even at threshold. The step structure observed in $N_R^0(E)$ is now seen as a natural consequence of the dynamics for the reverse reaction. For sufficiently high j, a large $P_R(j)$ switches-on instantly at threshold due to the adiabatic well. This effect is so strong as to survive in the highly averaged $N_R^0(E)$.

Discussion and Conclusions

The success of the simple adiabatic model confirms the proposition that the rotational enhancement effect is primarily due to straightforward RT dynamics in the entrance channel. The detailed structure of the reaction probabilities is found to also depend on the RT dynamics of the exit channel due to threshold effects. The fast vibration motion is not essential to the enhancement nor to most other (classically allowed) aspects of the reaction dynamics. The profiles of the reaction probabilities versus energy are mainly determined by the response of the barrier crossing probability ($P_\times$) to the details of the dynamics for the slow degrees of freedom. The fast vibration merely determines the adiabatic potential and sets the value of the nearly constant transmission coefficient κ. As a corollary, the bending zero point energy of the transition state does not contribute to the observed reaction threshold since the rotation/bending motion is actually more like translational motion in surmounting the barrier. While it is perhaps not surprising that an early TS system such as F + HCl is driven by the RT dynamics, we note that the adiabatic model described here is not restricted to such systems. Indeed, this model was very accurate for the symmetric I + HI reaction and can even be successfully used for the late TS system, Cl + HF.

The classical trajectory representation of these RT dynamics is completely adequate to make semiquantitative predictions of the enhancement effect and also provides a simple physical interpretation. The physical picture behind the enhancement effect is similar to the view developed in our earlier treatment of the I + HI reaction. Also, the study of Smith and coworkers[36,37] of the enhancement effect for O(^{3}P) + HCl using the KMM approximation have generated a model that quantifies the geometrical enhancement effect. However, the present study illustrates that straightline trajectories do not fully account for the rotational enhancement, since there is significant deflection by the entrance channel ridge. An advantage of the present adiabatic model is that once the time scale separation is invoked, the number of additional approximations is minimized since the full RT dynamics is considered. Moreover, reduced RT dynamics is easier to visualize and simulate than is the reaction in full dimensionality.

Of course, quantum mechanical effects in this reaction cannot be ignored. The system is replete with resonances, and the quantum tunneling is quite important at low energies. However, as we have previously demonstrated for I + HI, the adiabatic model provides a reasonable physical model of quantum reaction dynamics when implemented properly. The quantum resonance states can be fairly accurately represented by finding the bound and quasibound states in the vibrationally adiabatic potential wells. Furthermore, the full reaction dynamics (including tunneling) can be modeled through quantum rotational scattering, at least for symmetrical systems.

The transition state for the F + HCl reaction is highly bent. In light of the preceding discussion, we might expect that this feature would greatly promote the rotational enhancement effect. Somewhat surprisingly, this turns out not to be the case. In parallel with the present study of the DHSN−PES, we have also carried out preliminary studies of this reaction using a LEPS potential with a similar 3.8 kcal/mol barrier. The protruding ridge still exists on the adiabatic surface, but the saddlepoint lies at the collinear geometry. Dynamical simulations suggest that a comparable rotational enhancement effect also appears on the LEPS−PES. The geometrical (cone-of-acceptance) and stability attenuation effects do not appear to depend greatly on the location of the saddlepoint, which rather seem to reflect the overall shape of the protruding ridge.

Finally, we make several preliminary comparisons to other work on the F + HCl reaction. Quantum reaction probabilities have been computed by Tang et al.[22] on the low barrier, empirical Sayos−PES. The quantum wave packet calculations revealed the rotational enhancement effect exists on that surface but is somewhat weaker than observed for the DHSN−PES. We speculate that the lower barrier leads to a less prominent protruding ridge and hence to less angular deflection of the incoming flux. However, Tang et al.[22] did note the preference for large bend angle attack, which is qualitatively consistent with the view of the reaction dynamics presented here. This rotational enhancement therefore appears to be a more generic behavior, not crucially dependent on detailed aspects of the potential surface. Tang et al.[22] found no traces of the resonance structure in the reaction probabilities that we observed in the quantum calculations, although it is not clear whether their resolution was adequate to locate these narrow features. The vibrational product distribution obtained using QCT simulation by Sayos et al.[21] are peaked at HF($v' = 2$) rather than in HF($v' = 3$), as obtained here for low impact parameters. Experiment has likewise demonstrated that HF($v' = 2$) represents the largest product channel under thermal[14] conditions, with significant peaking in HF($v' = 2$, $j' \approx 10$). Interestingly, recent crossed jet studies of this reaction[18] under rigorously single collision conditions have revealed a surprising *bimodal* distribution for HF($v'=1, 2; j'$) peaking at both low ($j \approx 3$) and high ($j \approx 10$) rotational states, which suggests the presence of more than one dynamical pathway. A detailed comparison between quantum state resolved experimental results and quantum dynamical predictions from the DHNS−PES would be clearly interesting to pursue, as will be presented elsewhere.[28]

Acknowledgment. This work was supported by Academia Sinica, the National Research Council of Taiwan, the U.S. Air Force Office of Scientific Research, and the U.S. National Science Foundation. M.P.D. gratefully acknowledges graduate fellowship support from the Optical Sciences and Engineering Program, administered by the National Science Foundation.

References and Notes

(1) Skodje, R. T. *Annu. Rev. Phys. Chem.* **1993**, *44*, 145.
(2) Zhang, R.; van der Zande, W. J.; J. Bronikowski, M.; Zare, R. N. *J. Chem. Phys.* **1990**, *94*, 2704.
(3) Davis, M. J.; Koizumi, H.; Schatz, G. C.; Bradforth, S. E.; Neumark, D. M. *J. Chem. Phys.* **1994**, *101*, 4708.
(4) Moribayashi, K.; Nakamura, H. *J. Phys. Chem.* **1995**, *99*, 15410.
(5) Wang, L.; Kalyanaraman, C.; McCoy, A. B. *J. Chem. Phys.* **1999**, *110*, 11221.
(6) Ramachandran, B.; Schrader, E. A.; Senekowitsch, J.; Wyatt, R. E. *J. Chem. Phys.* **1999**, *111*, 3862.
(7) Skokov, S.; Tsuchida, T.; Nanbu, S.; Bowman, J. M.; Gray, S. K. *J. Chem. Phys.* **2000**, *113*, 227.
(8) Nobusada, K.; Nakamura, H.; Lin, Y.; Ramachandran, B. *J. Chem. Phys.* **2000**, *113*, 1018.
(9) Lin, Y.; Ramachandran, B.; Nobusada, K.; Nakamura, H. *J. Chem. Phys.* **2001**, *114*, 1549.
(10) Skokov, S.; Zou, S. L.; Bowman, J. M.; Allison, T. C.; Truhlar, D. G.; Lin, Y. J.; Ramachandran, B.; Garrett, B. C.; Lynch, B. J. *J. Phys. Chem. A* **2001**, *105*, 2298.

(11) Xie, T.; Wang, D. Y.; Bowman, J. M.; Manolopoulos, D. E. *J. Chem. Phys.* **2002**, *116*, 7461.
(12) Xie, T.; Bowman, J. M.; Peterson, K. A.; Ramachandran, B. *J. Chem. Phys.* **2003**, *119*, 9601.
(13) Xie, T.; Bowman, J. M.; Duff, J. W.; Braunstein, M.; Ramachandran, B. *J. Chem. Phys.* **2005**, *122*, 014301.
(14) Ding, A. M. G.; Kirsch, L. J.; Perry, D. S.; Polanyi, J. C. *Faraday Discuss. Chem. Soc.* **1973**, *55*, 252.
(15) Würzberg, E.; Houston, P. L. *J. Chem. Phys.* **1983**, *72*, 5915.
(16) Tamagake, K.; Setser, D. W.; Sung, J. P. *J. Chem. Phys.* **1980**, *73*, 2203.
(17) Moore, C. M.; Smith, I. W. M.; Stewart, D. W. A. *Int. J. Chem. Kinet.* **1994**, *26*, 813.
(18) Zolot, A.; Nesbitt, D. J. Manuscript in preparation.
(19) Last, I.; Baer, M. *J. Chem. Phys.* **1984**, *80*, 3246.
(20) Sayos, R.; Hernando, J.; Hijazo, J.; Gonzales, M. *Phys. Chem. Chem. Phys.* **1999**, *1*, 947.
(21) Sayos, R.; Hernando, J.; Francia, R.; Gonzales, M. *Phys. Chem. Chem. Phys.* **2000**, *2*, 523.
(22) Tang, B. Y.; Yang, B. H.; Han, K. L.; Zhang, R. Q.; Zhang, J. Z. H. *J. Chem. Phys.* **2000**, *113*, 10105.
(23) Kornweitz, H.; Persky, A. *J. Phys. Chem.* **2004**, *108*, 140.
(24) Deskevich, M. P.; Hayes, M. Y.; Skodje, R. T.; Nesbitt, D. J. Manuscript in preparation.
(25) Ramachandran, B.; Peterson, K. A. *J. Chem. Phys.* **2003**, *119*, 9590.
(26) Peterson, K. A.; Woon, D. E.; Dunning, T. H. *J. Chem. Phys.* **1994**, *100*, 7410.
(27) Aguado, A.; Paniagua, M. *J. Chem. Phys.* **1992**, *96*, 1285.
(28) Hayes, M. Y.; Takahashi, K.; Deskevich, M. P.; Nesbitt, D. J.;. Skodje, R. T. Manuscript in preparation.
(29) Sathyamurthy, N. *Chem. Rev.* **1983**, *83*, 601.
(30) Levine, R. D.; Bernstein, R. B.; *Chem. Phys. Lett.* **1984**, *105*, 467.
(31) Loesch, H. J. *Chem. Phys.* **1986**, *104*, 213.
(32) Skodje, R. T. *J. Chem. Phys.* **1991**, *95*, 7234.
(33) Grayce B. B.; Skodje, R. T. *J. Chem. Phys.* **1991**, *95*, 7249.
(34) Grayce, B. B.; Skodje, R. T. *J. Phys. Chem.* **1992**, *96*, 4134.
(35) Grayce, B. B.; Skodje, R. T.; Hutson, J. M. *J. Chem. Phys.* **1992**, *98*, 3929.
(36) Perdih, M.; Miklacv, A.; Smith, I. W. M. *J. Chem. Phys.* **1997**, *106*, 5478.
(37) Miklacv, A.; Perdih, M.; Smith, I. W. M. *J. Chem. Phys.* **2000**, *112*, 8813.
(38) Werner, H.-J.; et al. *MOLPRO*, version 2002.6.
(39) Deskevich, M. P.; Nesbitt, D. J.; Werner, H. J. *J. Chem. Phys.* **2004**, *120*, 7281.
(40) Skouteris, D.; Castillo, J. F.; Manolopoulos, D. E. *Comput. Phys. Commun.* **2000**, *133*, 128.
(41) Weaver, A.; Metz, R. B.; Bradforth, S. E.; Neumark, D. M. *J. Phys. Chem.* **1988**, *92*, 5558.
(42) Metz, R. B.; Weaver, A.; Bradforth, S. E.; Kitsopoulos, T. N.; Neumark, D. M.; *J. Phys. Chem.* **1990**, *94*, 1377.
(43) Bradforth, S. E.; Arnold, D. W.; Metz, R. B.; Weaver, A.; Neumark, D. M. *J. Phys. Chem.* **1991**, *95*, 8066.
(44) González-Sánchez, L.; Gómez-Carrasco, S.; Aguado, A.; Paniagua, M.; Hernández, M. L.; Alvariño, J. M.; Roncero, O. *J. Chem. Phys.* **2004**, *121*, 309.
(45) Skodje, R. T.; Yang, X. *Int. Rev. Phys. Chem.* **2004**, *23*, 253.
(46) Babamov, V. K.; Marcus, R. A. *J. Chem. Phys.* **1981**, *74*, 1790.
(47) Bondi, D. K.; Connor, J. N. L.; Manz, J.; Romelt, J. *Mol. Phys.* **1983**, *50*, 467.
(48) Kubach, C.; Rougeau, N. *J. Mol. Struct.−THEOCHEM* **1998**, *424*, 171.
(49) Bondi, D. K.; Connor, J. N. L.; Garrett, B. C.; Truhlar, D. G. *J. Chem. Phys.* **1983**, *78*, 5981.
(50) Aquilanti, V.; Grossi, G.; Lagana, A. *Chem. Phys. Lett.* **1982**, *81*, 179.
(51) Nobusada, K.; Tolstikhin, O. I.; Nakamura, H. *J. Chem. Phys.* **1998**, *108*, 8922.
(52) Skodje, R. T.; Davis, M. J. *J. Chem. Phys.* **1988**, *88*, 2429.
(53) (a) Cary, J. R.; Skodje, R. T. *Physica D* **1989**, *36*, 287. (b) Cary, J. R.; Skodje, R. T. *Phys. Rev. Lett.* **1988**, *61*, 1795.
(54) Skodje, R. T. *J. Chem. Phys.* **1989**, *90*, 6193.
(55) Davis, M. J.; Skodje, R. T. *Adv. Classical Trajectory Methods* **1992**, *1*, 77.
(56) Clary, D. C. *Mol. Phys.* **1984**, *53*, 3.